THE UNIVERSITY of EDINBURGH

Edinburgh Research Explorer

Origin of the Incommensurate Modulation in Te-III and Fermi-Surface Nesting in a Simple Metal

Citation for published version:
Loa, I, McMahon, M & Bosak, A 2009, 'Origin of the Incommensurate Modulation in Te-III and Fermi-Surface Nesting in a Simple Metal', *Physical Review Letters*, vol. 102, no. 3, 035501, pp. -. https://doi.org/10.1103/PhysRevLett.102.035501

Digital Object Identifier (DOI):
10.1103/PhysRevLett.102.035501

Link:
Link to publication record in Edinburgh Research Explorer

Document Version:
Publisher's PDF, also known as Version of record

Published In:
Physical Review Letters

Publisher Rights Statement:
Publisher's Version/PDF: author can archive publisher's version/PDF

General rights
Copyright for the publications made accessible via the Edinburgh Research Explorer is retained by the author(s) and / or other copyright owners and it is a condition of accessing these publications that users recognise and abide by the legal requirements associated with these rights.

Take down policy
The University of Edinburgh has made every reasonable effort to ensure that Edinburgh Research Explorer content complies with UK legislation. If you believe that the public display of this file breaches copyright please contact openaccess@ed.ac.uk providing details, and we will remove access to the work immediately and investigate your claim.

Download date: 07. May. 2023

Origin of the Incommensurate Modulation in Te-III and Fermi-Surface Nesting in a Simple Metal

I. Loa,[1,*] M. I. McMahon,[1] and A. Bosak[2]

[1]SUPA, School of Physics and Astronomy, Centre for Science at Extreme Conditions, The University of Edinburgh, Mayfield Road, Edinburgh, EH9 3JZ, United Kingdom

[2]European Synchrotron Radiation Facility, BP 220, 38043 Grenoble Cedex, France

(Received 4 September 2008; published 20 January 2009)

Inelastic x-ray scattering experiments have been performed on incommensurately modulated Te-III at high pressure and reveal a pronounced phonon anomaly. The anomaly is reproduced in first-principles lattice dynamics calculations of unmodulated, body-centered monoclinic (bcm) Te, which is shown to be dynamically unstable. The calculated Fermi surface of bcm Te exhibits surprisingly effective nesting for a simple, electronically three-dimensional metal. The combined experimental and theoretical results corroborate recent proposals that the modulated crystal structure of Te-III and other chalcogens is the manifestation of a pressure-induced charge-density wave state.

DOI: 10.1103/PhysRevLett.102.035501 PACS numbers: 61.44.Fw, 62.50.−p, 63.20.D−, 78.70.Ck

A wide range of inorganic and organic compounds [1–3] and even a protein [4] are known to possess incommensurately modulated (IM) crystal structures. The modulation breaks the translational symmetry of the crystal while preserving its long-range order. Such materials have been studied in great detail because of their unusual physical properties and because their discovery challenged the understanding of what constitutes a crystal. In recent years, IM crystal structures have been discovered, rather unexpectedly, in several pure elements at high pressure, namely, in I and Br [5,6], in Te, Se, and S [7–9], and in P [10]. Significant progress has been made in determining the detailed crystal structures of these phases, but the understanding of their physical properties and the mechanisms that lead to their formation is still fragmentary.

All of the above elements undergo pressure-induced metallization before they adopt their IM structures. In IM *metallic compounds*, the modulations are thought to be driven generally by the combination of sufficiently strong electron-phonon coupling and Fermi-surface (FS) nesting [1]. This leads to a softening of phonons with wave vectors corresponding to the nesting vector, known as a Kohn anomaly [11]. If the softening of a particular phonon is so large that its frequency becomes zero, the associated atomic displacements turn into a static modulation of the structure. This transition is associated with, and inseparable from, an instability of the electronic system towards a charge redistribution, and hence the new ground state is commonly called a charge-density wave (CDW) state. CDW states have been observed almost exclusively in electronically quasi-one- or quasi-two-dimensional systems. This appears to result from the fact that FS nesting can be realized much more easily in low-dimensional systems—where the electronic bands are nearly dispersionless in one or two directions—than in a three-dimensional (3D) metal. A notable exception is α-uranium, which is the only elemental metal known to adopt a modulated crystal structure at ambient pressure, but only below 43 K [12]. In α-U, the formation of a CDW hinges on the nesting of narrow f electron bands [13].

The situation in the chalcogens S, Se, and Te, all of them adopting the same modulated structure at high pressure and room temperature, is very different in that neither are they very anisotropic nor have they flat bands similar to the f-electron bands in α-U. It has been proposed recently [14,15] that the structural modulations in S, Se, and Te at high pressure are driven by the same mechanism as in the CDW compounds, while shear-wave instabilities have been pointed out as an important factor in Br and I [16,17]. There is, however, a complete lack of experimental data on the lattice dynamical and elastic properties to test these proposals. And on the theoretical side, recent work indicates that FS nesting exists in S at high pressure [15], but it remains unclear how it is possible to have effective FS nesting in simple, electronically 3D metals.

We present here results of inelastic x-ray scattering (IXS) experiments on incommensurately modulated Te-III at high pressure. The central result is the observation of a pronounced anomaly in the longitudinal-acoustic (LA) phonon branch at wave vectors close to that of the structural modulation. Complementary first-principles calculations show that both the experimentally observed phonon anomaly and the structural modulation of Te-III are directly related to a lattice dynamical instability in body-centered monoclinic Te (bcm Te), i.e., the unmodulated structure underlying that of Te-III [Fig. 1(a)]. Finally, the Fermi surface of bcm Te is determined from first-principles band structure calculations and is shown to exhibit surprisingly effective Fermi-surface nesting.

The IXS experiments were performed on beam line ID28 at the ESRF, Grenoble. The incident radiation was monochromatized at a photon energy of 17.794 keV. Two grazing-incidence mirrors focused the x rays onto the sample with a focal size of 30×60 μm^2. The spectrum of the scattered radiation was analyzed by a high-resolution spherical Si crystal analyzer to yield an overall

 © 2009 The American Physical Society

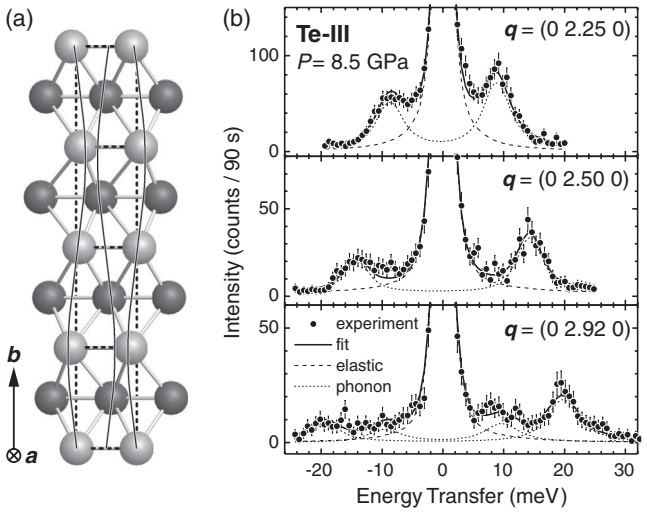

FIG. 1. (a) Crystal structure of Te-III. The dashed lines indicate four bcm unit cells, light and dark atoms are near the unit cell corners and centers, respectively, cylinders connect nearest neighbors, and solid lines highlight the modulation. (b) IXS spectra of Te-III at 8.5 GPa ($T = 295$ K) for three different momentum transfers q. The circles indicate the measured intensities, the lines denote the fitted spectra and the contributing components.

energy resolution of 3 meV. The momentum resolution was set to 0.4 nm^{-1}, and the IXS spectra were collected in the energy-scanning mode. A detailed account of the IXS setup has been given elsewhere [18].

In order to obtain a single crystal of Te-III with optimal dimensions for the IXS experiment, 70 pieces of Te were screened by x-ray diffraction for their crystal quality. About a third of them were pressurized in a diamond anvil pressure cell, using a 4:1 methanol-ethanol mixture as the pressure-transmitting medium. All of these ''large'' crystals of typically $100 \times 100 \times 40$ μm^3 broke apart at the structural phase transitions. Eventually, a relatively small crystal with satisfactory quality was chosen that had been used previously in structural studies [7]. The lateral dimensions of the crystal were 45×30 μm^2 with an estimated thickness of 10–20 μm. The Te-III crystal had two twin components [7], but the particular nature of the twinning is such that the reciprocal-space $(0\xi 0)$ lines of the twins coincide almost perfectly. Dispersion curves measured along this line are thus not affected by the twinning.

First-principles lattice dynamics calculations were performed in the framework of density functional theory using pseudopotentials, planes waves, linear response theory, and the generalized gradient approximation (GGA) [19] as implemented in the ABINIT code [20,21]. The Fermi surface of bcm Te was determined from electronic structure calculations using the full-potential, augmented plane-wave WIEN2K code [22] in the GGA and with a very dense mesh of 10^6 k points in the Brillouin zone. Both sets of calculations were performed for bcm Te using the experimental lattice parameters of Te-III at 8.5 GPa [7].

Figure 1(b) shows selected IXS spectra of Te-III at 8.5 GPa recorded for momentum transfers $\boldsymbol{q}$ parallel to the modulation vector $\boldsymbol{q}_m = 0.71\boldsymbol{b}^*$. The reciprocal lattice vector $\boldsymbol{b}^*$ refers to the reciprocal lattice derived from the conventional body-centered monoclinic description of the basic, i.e., unmodulated, structure of Te-III. We will use this $I2/m$ setting of space group $C2/m$ (#12) throughout the Letter to remain consistent with previous work [7]. Most of the spectra comprise the Stokes and anti-Stokes line of one dominant excitation in addition to the elastic line. Some of the spectra show additional weak structures, the origin of which is uncertain [the $\boldsymbol{q} = (0\ 2.92\ 0)$ spectrum in Fig. 1(b) is an example]. Also shown in Fig. 1(b) are decompositions of the measured spectra into the elastic line, the excitation peaks, and a constant background that were obtained by least-squares fitting [23]. The elastic and phonon lines were modeled as Lorentzian peaks and convoluted with the spectral resolution function of the spectrometer. The Stokes/anti-Stokes intensity ratios were assumed to be given by the Bose-Einstein population factors.

Figure 2(a) shows the momentum dependence of the measured phonon frequencies. The dominant features form a dispersive branch that can be attributed to the LA phonon branch on the basis of the IXS selection rules. This phonon branch exhibits the periodicity of the bcm lattice underlying the modulated structure of Te-III, and it shows a clear deviation from a sine-type dispersion

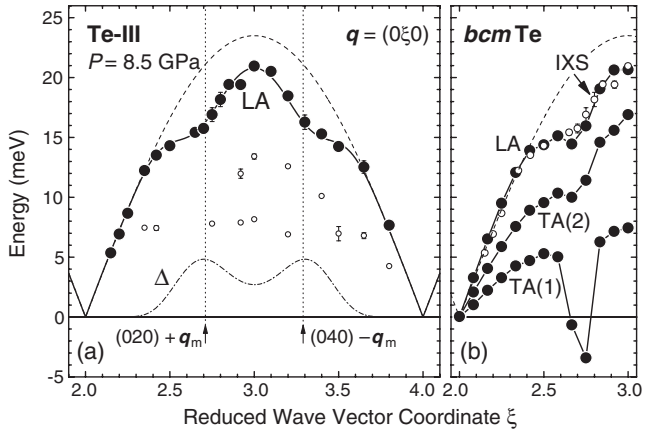

FIG. 2. (a) Measured phonon dispersion relation of Te-III at 8.5 GPa for momentum transfers $\boldsymbol{q} = (0\xi 0)$ parallel to the modulation vector. The solid symbols represent the results for the LA phonon dispersion branch, and small open symbols mark additional weak features observed in the IXS spectra. The solid line is a guide to the eye; the dashed line shows a sine-type dispersion relation and the dash-dotted line Δ shows the difference between the sine-type dispersion and the observed LA dispersion. (b) Calculated phonon dispersion curves of bcm Te (solid symbols). Phonons with imaginary frequencies are displayed with negative energies. The experimental results for the LA phonon branch in Te-III at 8.5 GPa are shown by small open symbols.

[dashed line in Fig. 2(a)] with depressions around (020) + $\boldsymbol{q}_m$ and (040) − $\boldsymbol{q}_m$.

The structural modulation in Te-III is transverse, and the corresponding transverse acoustic (TA) branch is expected to exhibit an even more pronounced anomaly than the LA branch. Despite the twinning of the crystal, an effort was made to obtain information on the TA branches, and the amplitudon and phason modes, by measuring IXS spectra along the $[0\xi 1]$ and $[0\xi\bar{2}\bar{2}]$ directions. But in this case the peak overlap in the measured spectra was too severe to permit the determination of reliable dispersion curves.

To examine the origin of both the observed LA phonon anomaly and the structural modulation in Te-III, lattice dynamical calculations were performed for the unmodulated bcm basic structure of Te-III. Figure 2(b) shows the calculated phonon dispersion curves in the $[0\xi 0]$ direction of bcm Te. The results for the LA branch are in excellent agreement with the experimental data. The calculated frequencies of the TA(1) branch are imaginary near the modulation wave vector, evidencing a dynamical instability of bcm Te. In other words, the energy landscape has a saddle point for the bcm equilibrium atomic positions, and the total energy of the crystal can be lowered by modulating the structure in the form of the TA(1) phonon mode. The calculated atomic displacement vector $\boldsymbol{u} = (u_x, 0, u_z)$ associated with the TA(1), $\boldsymbol{q} = (0, 2.75, 0)$ phonon has $u_z/u_x = 4.39$, which agrees with the value 4.30(21) observed experimentally for the static modulation in Te-III [7]. This shows unequivocally that the incommensurate structural modulation in Te-III results from the soft TA (1) mode in the dynamically unstable bcm Te.

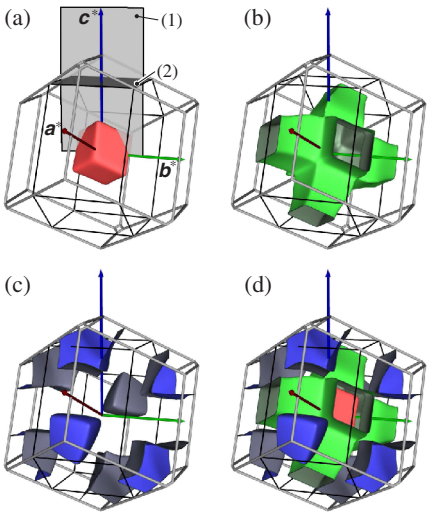

FIG. 3 (color online). Calculated Fermi surface of bcm Te, which comprises three sheets shown individually in (a)–(c) and combined in (d). Thick light-gray lines show the edges of the Brillouin zone, while the thin dark lines mark the Wigner-Seitz cell derived from the conventional bcm crystallographic unit cell. The reciprocal lattice vectors refer to the conventional bcm unit cell.

To elucidate the origin of the dynamical instability and its possible relation to FS nesting, we have calculated the Fermi surface of bcm Te. It consists of three sheets as shown in Fig. 3. The FS sheets in Figs. 3(a) and 3(b) have flat and parallel sections susceptible to nesting, but nesting related to the modulation vector $\boldsymbol{q}_m = 0.71\boldsymbol{b}^*$ is not discernable. However, nesting becomes clearly visible in the FS cross section in the $\boldsymbol{b}^*\boldsymbol{c}^*$ plane when all three sheets are considered together [Fig. 4(a)]. In this particular plane, the three sheets complement each other such that they form parallel and nearly straight FS lines, which are nested by $\boldsymbol{q}_m$. In fact, these sets of parallel lines can be nested by a whole range of vectors, but $\boldsymbol{q}_m$ is unique in that it connects two of the three sets of parallel lines simultaneously, which is illustrated schematically in the inset of Fig. 4(a). This situation is similar to what has been described as ''hidden Fermi-surface nesting'' in quasi-2D CDW systems such as the purple bronzes AMo_6O_{17} (A = Na, K) [24].

Band dispersion in all three spatial directions usually prevents efficient FS nesting, even if it exists in a particular plane in reciprocal space. Figure 4(b) shows the FS cross section of bcm Te in the plane perpendicular to $\boldsymbol{c}^*$ and passing through $\frac{1}{2}\boldsymbol{c}^*$ [marked as plane (2) in Fig. 3(a)], which is perpendicular to the $\boldsymbol{b}^*\boldsymbol{c}^*$ plane discussed so far.

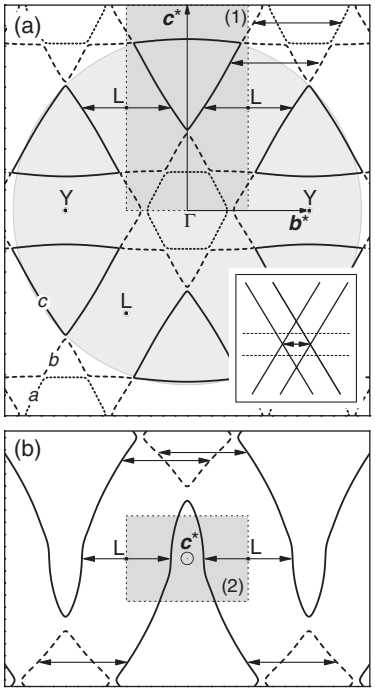

FIG. 4. Calculated Fermi surface of bcm Te (a) in the $\boldsymbol{b}^*\boldsymbol{c}^*$ plane through Γ and (b) in the (001) plane through $\frac{1}{2}\boldsymbol{c}^*$. The gray-shaded rectangles are the same as shown in Fig. 3(a). Dotted, dashed, and solid lines correspond to the FS sheets shown in Figs. 3(a)–3(c), respectively. The inset in (a) illustrates the idealized parallel sections of the Fermi surface and the ''double nesting'' of two sets of FS sheets with the same nesting vector. The gray-shaded circle shows the size of the free-electron Fermi sphere.

In plane (2), the FS lines are more curved than in the b^*c^* plane, but there are still extended parallel sections that are nested by $\boldsymbol{q}_m$. In planes parallel to the planes (1) and (2), but offset from these, the nesting becomes less complete, but altogether a sizeable fraction of the FS is nested by $\boldsymbol{q} \approx \boldsymbol{q}_m$. Furthermore, the nesting occurs generally between parts of the FS with Fermi velocities of opposite sign, so that not only states at the Fermi level take part but also states somewhat above and below (see Ref. [25] for a discussion of this effect). Given that bcm Te it is not a quasi-1D or 2D electronic system, its Fermi surface exhibits surprisingly effective nesting.

In comparison, the FS in the free-electron approximation (not shown), derived from Fermi spheres, has a more complex topology and is less susceptible to nesting. The differences are largely due to the electron-ion interaction, i.e., the standard band structure effect of opening energy gaps at the Brillouin zone boundary. This removes parts of the sheets c and reduces the curvature of sheets a and b so that the straight, highly nested sections appear [Fig. 4(a)].

The FS of bcm Te is sensitive to small distortions of the crystal unit cell: Increasing the monoclinic angle β by only 3° results in a significantly larger length variation of the nesting vector in the b^*c^* plane and hence less effective nesting. Likewise, the free-electron FS depends on the shape of the unit cell, but not on its volume. The Fermi-surface nesting calculated for bcm Te is therefore expected to exist in similar form in the analog bcm phases of Se and S. This would explain why the IM phases of S, Se, and Te all have the same underlying bcm lattice and that the ratios of the lattice parameters agree within 2% and the monoclinic angles within 0.4° at the lowest pressures of their respective stability ranges. It appears that it is this particular unit cell geometry, paired with a ''generic'' nearly free-electron band structure, that gives rise to strong Fermi-surface nesting in these simple 3D metals.

In conclusion, IXS experiments on high-pressure Te-III have revealed a pronounced phonon anomaly near wave vectors corresponding to the incommensurate modulation wave vector. The anomaly in the LA branch is reproduced in first-principles lattice dynamics calculations of bcm Te, which is shown to be dynamically unstable. The atomic displacements associated with the unstable TA phonon mode in bcm Te agree with those observed experimentally as the static modulation in Te-III. The calculated Fermi surface of bcm Te exhibits surprisingly effective nesting for a simple 3D metal, and the dominant nesting vector agrees with the experimentally observed modulation vector. Taking into account also theoretical results on the electron-phonon coupling in bcm S [15], it leads us to conclude that Te-III is indeed a CDW system, driven by the combination of electron-phonon coupling and FS nesting as proposed for S, Se, and Te [14,15]. The role of high pressure is (i) to metallize the material and (ii) to increase its density so that more close-packed structures such as body-centered monoclinic and cubic become energetically favorable. Not only do these results provide a coherent picture of the mechanism that leads to the IM crystal structure of Te-III and other chalcogens at high pressure, but they are also at variance with recent work by Johannes and Mazin [25] who challenge the common view that FS nesting plays an important role in the formation of a CDW state.

We thank S. R. Evans and O. Degtyareva for help with the experiment and C. Hejny for producing the Te crystal. Supported by grants from the UK Engineering and Physical Sciences Research Council, and facilities were made available by the European Synchrotron Radiation Facility and Daresbury Laboratory.

*Corresponding author.
I.Loa@ed.ac.uk

[1] G. Grüner, *Density Waves in Solids, Frontiers in Physics* (Perseus Publishing, Cambridge, USA, 1994).
[2] *Incommensurate Phases in Dielectrics*, edited by R. Blinc and A. P. Levanyuk, Modern Problems in Condensed Matter Sciences Vol. 14 (North Holland Physics, Amsterdam, 1986).
[3] H. Cummins, Phys. Rep. **185**, 211 (1990).
[4] J. J. Lovelace *et al.*, J. Appl. Crystallogr. **41**, 600 (2008).
[5] K. Takemura, K. Sato, H. Fujihisa, and M. Onoda, Nature (London) **423**, 971 (2003).
[6] T. Kume *et al.*, Phys. Rev. Lett. **94**, 065506 (2005).
[7] C. Hejny and M. I. McMahon, Phys. Rev. Lett. **91**, 215502 (2003).
[8] M. I. McMahon *et al.*, Phys. Rev. B **70**, 054101 (2004).
[9] C. Hejny *et al.*, Phys. Rev. B **71**, 020101(R) (2005).
[10] H. Fujihisa *et al.*, Phys. Rev. Lett. **98**, 175501 (2007).
[11] W. Kohn, Phys. Rev. Lett. **2**, 393 (1959).
[12] H. G. Smith *et al.*, Phys. Rev. Lett. **44**, 1612 (1980).
[13] L. Fast *et al.*, Phys. Rev. Lett. **81**, 2978 (1998).
[14] G. J. Ackland and H. Fox, J. Phys. Condens. Matter **17**, 1851 (2005).
[15] O. Degtyareva *et al.*, Phys. Rev. Lett. **99**, 155505 (2007).
[16] D. Duan *et al.*, Phys. Rev. B **76**, 104113 (2007).
[17] X. San *et al.*, J. Phys. Condens. Matter **20**, 175225 (2008).
[18] M. Krisch, J. Raman Spectrosc. **34**, 628 (2003).
[19] J. P. Perdew, K. Burke, and M. Ernzerhof, Phys. Rev. Lett. **77**, 3865 (1996).
[20] X. Gonze *et al.*, Comput. Mater. Sci. **25**, 478 (2002); http://www.abinit.org.
[21] GGA-type Fritz-Haber-Institute (FHI) pseudopotentials were used. The full Brillouin zone was sampled at 1920 k-points, and the k-point density was doubled along the b^* direction compared to a standard mesh to permit the calculation of a larger number of phonons along $(0\xi 0)$.
[22] P. Blaha *et al.*, *WIEN2K, An Augmented Plane Wave + Local Orbitals Program for Calculating Crystal Properties*, edited by K. Schwarz (Techn. Universität Wien, Austria, 2001).
[23] Computer Program FIT28, beam line ID28, ESRF.
[24] M.-H. Whangbo, E. Canadell, P. Foury, and J.-P. Pouget, Science **252**, 96 (1991).
[25] M. D. Johannes and I. I. Mazin, Phys. Rev. B **77**, 165135 (2008).